I.J. Image, Graphics and Signal Processing, **2024, 2, 29-42**
Published Online on April 8, 2024 by MECS Press (http://www.mecs-press.org/)
DOI: 10.5815/ijigsp.2024.02.03

Multifractal Scaling of Singularity Spectra of Digital Mueller-matrix Images of Biological Tissues: Fundamental and Applied Aspects

Oleksandr Ushenko
Research Institute of Zhejiang University-Taizhou, Taizhou, China
E-mail: o.ushenko@chnu.edu.ua
ORCID iD: https://orcid.org/0000-0001-7015-7423

Oleksandr Saleha
Optics and Publishing Department, Yuriy Fedkovych Chernivtsi National University, Chernivtsi, Ukraine
E-mail: o.salega@chnu.edu.ua
ORCID iD: https://orcid.org/0000-0002-0735-3920

Yurii Ushenko*
Computer Science Department, Yuriy Fedkovych Chernivtsi National University, Chernivtsi, Ukraine
E-mail: y.ushenko@chnu.edu.ua
ORCID iD: https://orcid.org/0000-0003-1767-1882
*Corresponding Author

Ivan Gordey
Computer Science Department, Yuriy Fedkovych Chernivtsi National University, Chernivtsi, Ukraine
hordei.ivan@chnu.edu.ua
ORCID iD: https://orcid.org/0000-0003-3179-0394

Oleksandra Litvinenko
Bucovinian State Medical University, Chernivtsi, Ukraine
E-mail: sawasawa901@gmail.com
ORCID iD: https://orcid.org/0000-0003-3897-6765

Received: 13 October, 2023; Revised: 16 November, 2023; Accepted: 24 December, 2023; Published: 08 April, 2024

Abstract: The fundamental component of the work contains a summary of the theoretical foundations of the algorithms of the scale-self-similar approach for the analysis of digital Mueller-matrix images of birefringent architectonics of biological tissues. The theoretical consideration of multifractal analysis and determination of singularity spectra of fractal dimensions of coordinate distributions of matrix elements (Mueller-matrix images - MMI) of biological tissue preparations is based on the method of maxima of amplitude modules of the wavelet transform (WTMM). The applied part of the work is devoted to the comparison of diagnostic capabilities for determining the prescription of mechanical brain injury using algorithms of statistical (central statistical moments of the 1st - 4th orders), fractal (approximating curves to logarithmic dependences of power spectra) and multifractal (WTMM) analysis of MMI linear birefringence of fibrillar networks of neurons of nervous tissue. Excellent (~95%) accuracy of differential diagnosis of the prescription of mechanical injury has been achieved.

Index Terms: Mueller matrix, biological tissue, optical anisotropy, birefringence, fractal, singularity spectrum, wavelet transform, diagnostics, trauma, spleen.

1. Introduction

Recently, within the framework of numerous studies in the field of biomedical polarimetry [1-7], digital methods for processing the obtained data - polarizing mapping [8,9], Mueller – matrix images [10-16], maps of optical

anisotropy [17,18] have been widely used. as a result, a number of objective criteria (markers) for detecting changes in the morphological structure of biological tissues caused by various pathological (cancer [19], endometriosis [20], inflammatory processes [21]) and necrotic (prescription of onset and differentiation of causes of death [22]) conditions. Statistical and correlation analysis of the biological preparation's polarization azimuth and ellipticity, Mueller matrix elements coordinate distributions is the predominant algorithmic basis for determining the totality of polarimetric digital diagnostic markers of the above conditions [23].

The effective implementation of digital algorithms in the biomedical polarimetry technique and practice has prompted new research aimed at expanding the statistical algorithmic base using singular (distribution of the number of polarization-singular states of the object field [24,25]) and scale-selective wavelet [26,27] and Fourier [28,29] approaches. The result was an expansion of the set of objective diagnostic markers and an improvement in the polarizing biomedical diagnostics methods sensitivity in oncology and gynecology [30,31].

A new step in expanding the functionality of biological preparations traditional 2D imaging polarimetry to 3D analysis was use phase scanning algorithms and complex amplitudes fields digital holographic reproduction [32-35].

At the same time, the functionality of 3D digital polarimetry was limited due to the lack of algorithms for obtaining and evaluating (inaccessible to statistical and correlation methods) the topological scale - self-similar information about the Mueller matrix images of orientation-phase topography of the architectonics of biological tissues. One of the possible ways to effectively overcome this biomedical diagnostics problem is use multifractal analysis or multifractal scaling [36-41].

Our article is aimed at studying the relationship between the scale-self-similar structure of maps of Mueller matrix images (multifractal spectra) and the phase topography of the architectonics of biological tissues in order to determine diagnostic markers of differentiation of necrotic changes prescription of mechanical spleen injury.

2. Brief Theory

2.1. "Phase" Mueller matrix images

We will conduct a brief theoretical analysis in the approximation of structural anisotropy (linear birefringence LB) of fibrillar protein networks, which are the basis of architectonics in most biological tissues [4-15].

Optical manifestations of this mechanism are characterized by a partial Mueller matrix$\{F_{LB}\}$

$$\{F_{LB}\} = \begin{Vmatrix} 1 & 0 & 0 & 0 \\ 0 & f_{22} & f_{23} & f_{24} \\ 0 & f_{32} & f_{33} & f_{34} \\ 0 & f_{42} & f_{43} & f_{44} \end{Vmatrix}, \tag{1}$$

where

$$f_{ik}(\gamma,\delta) = \begin{cases} f_{22} = cos^2 2\gamma + sin^2 2\gamma \cos\delta\,; \\ f_{23} = f_{32} = cos\,2\gamma \sin 2\gamma(1-\cos\delta); \\ f_{33} = sin^2 2\gamma + cos^2 2\gamma \cos\delta\,; \\ f_{42} = -f_{24} = sin\,2\gamma \sin\delta\,; \\ f_{34} = -f_{43} = cos\,2\gamma \sin\delta\,; \\ f_{44} = cos\,\delta\,. \end{cases} \tag{2}$$

Here γ – direction of optical axis; $\delta = \frac{2\pi}{\lambda}\Delta n l$ - phase shift between linearly orthogonally polarized components of the laser beam amplitude; λ – wavelength; Δn – birefringence value; l – geometrical thickness of biological layer.

Analysis of relations (1) and (2) shows, that almost all partial matrix elements $f_{ik}(\gamma,\delta)$ are azimuthally (γ) dependent.

This circumstance does not allow them to be used in serial and statistically reliable group measurements of biological tissue samples.

The exception is the so-called Muller matrix invariants $MMI_{ik}(\delta)$

$$MMI_{ik}(\gamma,\delta) \underset{\gamma=0}{\longrightarrow} \equiv f_{44}(\delta) = cos\delta; \tag{3}$$

$$MMI_{ik}(\gamma,\delta) \underset{\gamma=0}{\longrightarrow} \equiv f_{22} + f_{33} = 1 + cos\delta. \tag{4}$$

In the future, we will use as $MMI_{ik}(\delta)$ the coordinate distributions (m,n) of the matrix parameter $f_{44}(\delta)$ - will be called phase" Mueller-matrix images $f_{44}(m,n)$.

2.2. Multifractal scaling

We have already noted [36] that fractality is inherent not only in geometric structures, but also in various processes that can form scale-like distributions (fractal measures) – in our case, $f_{44}(m,n)$ of biological tissues histological sections.

It is known from the fractal's theory that such measures ($f_{44}(m,n)$) can be of two types – fractal $f_{44}(m,n)^h$ or multifractal $f_{44}(m,n)^{F(h)}$ For fractal distributions $f_{44}(m,n)^h$, the concepts of one fractal dimension $h \equiv h_0$ are introduced. Multifractal distributions $f_{44}(m,n)^{F(h)}$ are characterized by a set of fractal dimensions h_r or a singularities spectrum $F(h)$. To calculate the fractal dimensions of h_r, a special approach is used, which is clearly based on the introduction of partial functions or generalized statistical sums [39].

$$Z(r,d) = \sum_{i=1}^{P(d)} f_{44}(m,n)_j^r(d). \tag{5}$$

Here $P(d)$ – number of multifractal distribution coating elements $f_{44}(m,n)_j^r$; $r \in R$.

As a rule, the dependence (6) has a stepwise character

$$Z(r,d) \sim d^{(r-1)h_r} \tag{6}$$

where h_r – generalized fractal dimension, which for the case of partial functions is written as scaling exponents

$$\tau(r) = (r-1)h_r \tag{7}$$

Here, the exponent $(r-1)$ is introduced into the exponent in order to automatically fulfill the equality $Z(1,d) = 1$, which means the normalization conditions for the MMI distribution $f_{44}(m,n)_j^r(d)$.

In particular, for monofractals $\tau(r) = const$.

For more complex scale-like distributions, dependence (8) is transformed into a specific multifractal spectrum $F(h_r)$.

For analytical determination of the dependence $F(h_r)$, the method of wavelet transforms modules maxima WTMM [39 – 41] is used.

2.3. Method of wavelet transform modules maxima

Method WTMM includes two steps:

- Wavelet transformation $W(a,b)$ of the $f_{44}(m,n)$ set and the skeleton $sup|W(a^*, x_i(a^*))|$ determination - the maximum modulus local surface extremes values wavelet coefficients $W(a,b)$ lines for each scale a of scanning soliton-like function $V(b)$;
- Construction of wavelet coefficient modules $Z(r,d,sup|W(a^*,x_i(a^*))|)$ local maxima partial functions and fractal dimension spectrum $F(h_r)$ determination.

2.3.1. Wavelet transform $W(a,b)$

The $f_{44}(m,n)$ wavelet analysis (relations (3),(4)) is based on an analytical transformation consisting in the decomposition of a distribution over a basis constructed from a soliton-like function (wavelet) by means of large-scale changes and transfers [45,46].

The continuous wavelet transforms of the function $\omega_{ii}(x)$ is defined by the following formula

$$W(a,b) = \frac{1}{\sqrt{a}} \int_{-\infty}^{\infty} f_{44}(x) V\left(\frac{x-b}{a}\right) dx \tag{8}$$

where a is a scale parameter, b is a spatial coordinate, and V is a soliton–like function (wavelet) constructed on the basis of the Gaussian function derivatives.

In our work, the second derivative (m=2) or MHAT wavelet is used

$$V^{(m)} = (-1)^m \frac{\partial^m}{\partial x^m}\left[exp\left(\frac{x^2}{2}\right)\right] \Rightarrow V^{(2)} = \frac{\partial^2}{\partial x^2}\left[exp\left(\frac{x^2}{2}\right)\right] \tag{9}$$

The wavelet relations (9),(10) for MMI (ratio (5)) can be written as the following expressions

$$W^{\delta}(a,b) = \frac{1}{\sqrt{a}} \int_{-\infty}^{\infty} f_{44}(\delta,a,x) V\left(\frac{x-b}{a}\right) dx \tag{10}$$

The expressions (8) - (10) analysis shows that the wavelet decomposition of biological tissues samples is a superposition parameters multi - scale distributions (fractal or multifractal measures $f_{44_j}^{r}(d)$ of the optical anisotropic architectonics of the fibrillar network) - expression (10)).

In the following, we will focus on the search for the possibility's scaling exponents $\tau(r)$ (expression (7)) determination that characterize $f_{44_j}^{r}(d)$, based on the use of skeletons $sup|W(a^*, x_i(a^*))|$.

2.3.2. The fractal dimension spectrum $F(h_r)$ determination

This analytical procedure is based on the construction of partial functions using the following formula

$$Z(r,d) = \sum_{l \in L(a)} (sup|W(a^*, x_i(a^*))|)^r \quad (11)$$

According to [39-41], the following dependence $Z(r,d) \sim d^{\tau(r)}$ holds, where the fractal dimension $\tau(r)$ for some r is determined by setting the scaling exponent ${lnZ(r,d)}/{lnd}$ dependence slope.

Variation of r in construction $\sum_{l \in L(a)} (sup|W(a^*, x_i(a^*))|)^r$ allows you to get:

- for fractal distributions $f_{44_j}^{r}(d)$ line dependences $\tau(r)$, - $(h(r) = {d\tau}/{dr} = const)$;
- for multifractal distributions $f_{44_j}^{r}(d)$ none line dependences $\tau(r) = rh - D(h)$ with big number of fractal dimensions $h(r) = {d\tau}/{dr}$, which characterized the multifractal spectrum $F\big(h(r)\big)$.

In our case, we will study the multifractal spectra of $f_{44_j}^{r}(d)$ based on the partial functions $Z(r, d, sup|W(a^*, x_i(a^*))|)$ wavelet maximal modules amplitudes skeletons $sup|W(a^*, x_i(a^*))|$ for "phase" parameter of the fibrillar network – $(F^{\delta}(h_r))$.

3. The Experimental Setup and Measurement Methodology

A generalization of the polarization interferometry scheme [32-35] is the Mueller matrix mapping scheme on the base of Mach-Zehnder interferometer, which is shown in Fig. 1.

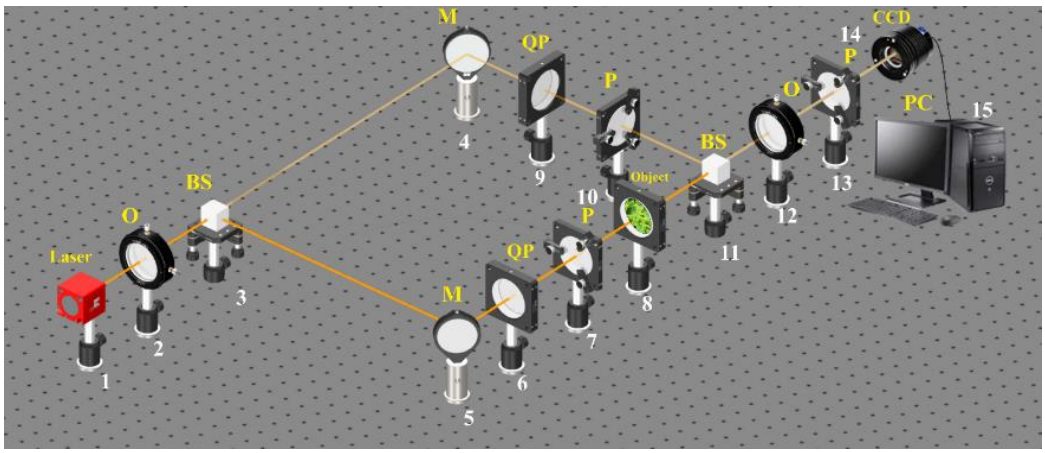

Fig. 1. Optical scheme for polarization-interference Mueller-matrix parameters mapping. 1 – He-Ne laser; 2 - collimator – "O"; 3,11 – beam splitters – "BS"; 4,5 – mirrors – "M"; 7,10,13 — polarizer's "P"; 6,9 – quarter wave plates – "QP"; 8 – object; 12 – polarization objective – "O"; 14 – digital camera – "CCD"; 15 – personal computer – "PC".

Parallel ($Ø = 2 \times 10^3 \mu m$) beam of He-Ne ($\lambda = 0.6328 \mu m$) laser 1, formed by spatial-frequency filter 2, with 50% beam splitter 3 is divided into "object" and "reference" ones.

The "object" beam with the help of a rotating mirror 5 is directed through the polarizing filter 6 - 7 in the direction of the spleen tissue 8 sample. The polarization-inhomogeneous image of spleen tissue 8 is projected by the strain-free objective 12 into the digital camera 14.

The "reference" beam is directed by the mirror 4 through the polarization filter 9 - 10 into the plane of polarization-inhomogeneous image histological section of spleen tissue 8.

As a result, an interference pattern is formed, the coordinate intensity distribution of which is recorded by a digital camera 14 through a polarizer 13.

Before carrying out measurements of spleen tissue, the experimental device passed metrological certification with the introduction of model objects ("clean air", "linear polarizer", "phase plates 0.25λ", "0.5λ"). As 50 measurements for each type of object, the errors were determined $\sim 1\% - 2\%$.

The methodology for layer-by-layer object field measurement using complex amplitudes E_x and E_y digital holographic reconstruction is presented in [33-35]. However, detailed information is not provided in this work.

For a better understanding of the further discussion, we will provide a brief overview of 3D digital holographic scanning method.

4. The method of 3D Mueller-matrix scanning of object field

The method of polarization-interference determination of "phase" element f_44 (δ) of the Mueller matrix consists in the following set of actions:

- Formation of two – "wright" $(\otimes - \otimes)$ and "left" $(\oplus - \oplus)$ circulary polarization states in irradiating and supporting laser beams.
- Recording of each partial interference pattern through the polarizer-analyzer 14 with a sequential orientation of the transmission plane at angles $\Omega = 0^0; \quad \Omega = 90^0$.
- Recovery for each partial interference distribution using a digital Fourier transform of the coordinate distributions of complex amplitudes $\{E_x(m,n); \quad E_y(m,n)\}$ of the object field in the biological layer plane [28,29,31-35]

$$E_{x;y}^{(\otimes-\oplus)} \Rightarrow FT_{x;y}(\upsilon,\nu) = \frac{1}{M\times N}\sum_{m=0}^{M-1}\sum_{n=0}^{N-1} I_{x,y}(\Omega = 0^0; 90^0)(m,n)\, exp\left[-i2\pi\left(\frac{m\times\upsilon}{M} + \frac{n\times\nu}{N}\right)\right] \tag{12}$$

where

$$\begin{cases} I_x^{(\otimes \ -\oplus \ )}(\Omega = 0^0)(m,n) = E_x^{(\otimes \ -\oplus \ )}(m,n)\left(E_x^{(\otimes \ -\oplus \ )}\right)^*(m,n); \\ I_y^{(\otimes \ -\oplus \ )}(\Omega = 90^0)(m,n) = E_y^{(\otimes \ -\oplus \ )}(m,n)\left(E_y^{(\otimes \ -\oplus \ )}\right)^*(m,n). \end{cases}$$

$E_{x,y}^{(\otimes-\oplus)}$ - orthogonal components of complex amplitudes for different orientations $\Omega = 0^0; \quad \Omega = 90^0$; $*$ - denotes the complex conjugation operation; (υ,ν) are the spatial frequencies and $(m = 1120, n = 960)$ are the quantity of pixels of the CCD camera .

- For each state of the irradiating beam, the distributions of the 4th parameters of Stokes vector of the object field of the biological layer are calculated using the reproduced distributions of complex amplitudes $\left\{E_x^{(\otimes-\oplus)}(m,n); E_y^{(\otimes-\oplus)}(m,n)\right\}$ using the following relations [4-9]

$$S_{4j}^{(\otimes-\oplus)} = i\left(E_x E_y^* - E_y E_x^*\right)_J^{(\otimes-\oplus)} \tag{13}$$

- Further, on the basis of relations (14), the elements f_{44} of the Mueller matrix is calculated using the following Stokes-polarimetric relations for right-and left-circularly polarized probe beams $S^0(\otimes); \quad S^0(\oplus)$:

$$\left\{\begin{array}{l} \left[S^0(\otimes) = \{F\}\begin{pmatrix}1\\0\\0\\1\end{pmatrix} \rightarrow S(\otimes) = \begin{pmatrix}f_{11}+f_{14}\\f_{21}+f_{24}\\f_{31}+f_{34}\\f_{41}+f_{44}\end{pmatrix}\right]; \\ \left[S^0(\oplus) = \{F\}\begin{pmatrix}1\\0\\0\\-1\end{pmatrix} \rightarrow S(\oplus) = \begin{pmatrix}f_{11}-f_{14}\\f_{21}-f_{24}\\f_{31}-f_{34}\\f_{41}-f_{44}\end{pmatrix}\right] \end{array}\right\} \Rightarrow f_{ik} = \left\|\begin{matrix} f_{11} & f_{14} \\ f_{21} & f_{24} \\ f_{31} & f_{34} \\ f_{41} & f_{44} \end{matrix}\right\| \tag{14}$$

From expressions (13) –(14), we obtain working relations for determining the values of f_{44} elements of the Mueller matrix

$$f_{44} = 0{,}5\left(S_4^{\otimes} - S_4^{\oplus}\right) \tag{15}$$

- To implement phase scanning of the volume of biological tissues the digital Fourier transforms results are used to obtain complex amplitudes distributions according to the following algorithms

$$\begin{cases} E_{0^0}^{\otimes-\oplus} \to |E_x^{\otimes-\oplus}(\Omega = 0^0)|; \\ E_{90^0}^{\Theta} \to \left|E_y^{\otimes-\oplus}(\Omega = 90^0)\right| exp\left(i\left(\varphi_y^{\otimes-\oplus} - \varphi_x^{\otimes-\oplus}\right)\right) \end{cases} \quad (16)$$

By means of stepwise ($\Delta\varphi$) phase (φ_k) scanning of the reconstructed field complex amplitudes (relations (12)) using algorithms (14)-(16) we obtain layer-by-layer phase Mueller matrix images $f_{44}(\varphi_k, m, n)$ different layers or depths in the volume of the histological section of biological tissue. For the $f_{44}(\varphi_k, m, n)$ apply the wavelet schedule $W^{\delta}(a, b)$ (equations (8), (9)).

- Determine the wavelet amplitudes maxima modules skeletons $sup|W(a^*, x_i(a^*))|$ for thesiograms of facies optical anisotropy, which serve as the basis for calculating multifractal spectra $F^{\delta}(h_i(r))$ by the WTMM method, - $Z(r, d, sup|W(a^*, x_i(a^*))|) \Leftrightarrow {lnZ(r,d)}/{_{lnd}}$.
- The resulting set of the MMI $f_{44}(\varphi_k, m, n)$ multifractal spectra $F(h_j)$ was analyzed in a statistical approach using the following algorithms to calculate mean (Z_1), variance (Z_2), skewness (Z_3) and kurtosis (Z_4) [24,25]

$$Z_1 = \frac{1}{K}\sum_{j=1}^{K} F(h_j);$$
$$Z_2 = \sqrt{\frac{1}{K}\sum_{j=1}^{K} F(h_j^2)};$$
$$Z_3 = \frac{1}{Z_2^3}\frac{1}{K}\sum_{j=1}^{K} F(h_j^3);$$
$$Z_4 = \frac{1}{Z_2^4}\frac{1}{K}\sum_{j=1}^{K} F(h_j^4)$$

where K – CCD pixels quantity.

5. Objects of Investigations

In our work, we will consider two types of biological tissues:

- Group 1 - spleen tissue with a mechanical injury duration of 6 hours (21 samples).
- Group 2 - spleen tissue with a mechanical injury duration of 24 hours (21 samples).

In order to exclude the depolarizing effect on the $f_{44}(m, n)$ structure of formalin and paraffin, native preparations of histological sections of the spleen of those who died were used for experimental studies.

Histological sections were made on a microtome with rapid freezing according to the standard procedure.

The optical-geometric parameters of histological sections of spleen tissues are presented in Table 1.

Table 1. Optical- geometric parameters of histological sections of spleen tissues

Parameters	$T = 6\ hours$ (21 samples)	$T = 24\ hours$ (21 samples)
Attenuation (extinction) coefficient τ, cm^{-1}	0.23±0.012	0.26±0.014
Depolarization degree $\Lambda, \%$	25 ± 1.21	34±2.15

The biological tissues samples extinction coefficient (τ, cm^{-1}) was measured according to the standard photometry illuminating beam intensity attenuation method [47] using an integral light-scattering sphere [48-50]. The spleen tissues samples integral depolarization degree ($\Lambda, \%$) measurement was carried out in the convenient Mueller-matrix polarimeter scheme [19-31].

Representative samples number sampling to determine the statistical significance by the cross-validation method[49]. The standard deviation σ^2 for all the statistical moments $Z_{i=1;2;3;4}(n)$ was determined. The specified samples number (21 for each group) provided the level $\sigma^2 \leq 0.025$. This standard deviation corresponds to a confidence interval $p < 0.05$, which demonstrates the statistical reliability of the 3D Mueller-matrix mapping and WTMM methods.

6. Experimental Results and Discussion

6.1. Statistical and fractal analysis

This part of the article presents the results of comparative statistical (Fig. 2 and Fig. 3, fragments (1)-(4)) and fractal (Fig. 2 and Fig. 3, fragments (5), (6)) analysis of the data of the Mueller matrix mapping of the "phase" invariants $f_{44}(\delta)$ of the architectonics of histological sections of the spleen (group 1 and group 2).

6.1.1. Spleen – statistical analysis

Fig. 2 illustrates maps (fragments (1), (2)), histograms (fragments (3),(4)) and logarithmic dependences of power spectra (fragments (5),(6)) of distributions $f_{44}(m,n)$, which characterize the phase structure of birefringent networks of the entire volume of the histological section of the spleen.

Fig. 3 shows similar dependences obtained by phase scanning (ratios (12)-(16)) for an optically thin (single scattering) layer of a histological slice of the spleen.

It is shown that the two-dimensional distributions of the "phase" invariants $f_{44}(m,n)$ of the optically anisotropic architectonics of histological sections of the spleen are coordinate-inhomogeneous, - Fig. 2, Fig. 3, fragments (1), (2).

Histograms $N(f_{44})$ are asymmetric and characterized by variously localized maxima, - Fig.2, Fig. 3, fragments (3),(4).

For the architectonics of the optically thin layer of the spleen ($\varphi_k = {}^{\pi}/_{8}$), there is a decrease in the range of variation of random values of phase invariants $f_{44}(\delta)$, - Fig. 3, fragments (3), (4).

Regardless of the prescription of mechanical injury to the spleen tissue, coordinate (m,n) and probabilistic $N(f_{44})$ distributions $f_{44}(m,n)$ sufficiently similar (Fig. 2 and Fig. 3, fragments (1), (3) and (2), (4)).

Quantitatively, histograms of distributions of random values of phase invariants $f_{44}(m,n)$ from both groups characterizes the totality of central statistical moments of the 1st - 4th orders, – table 2.

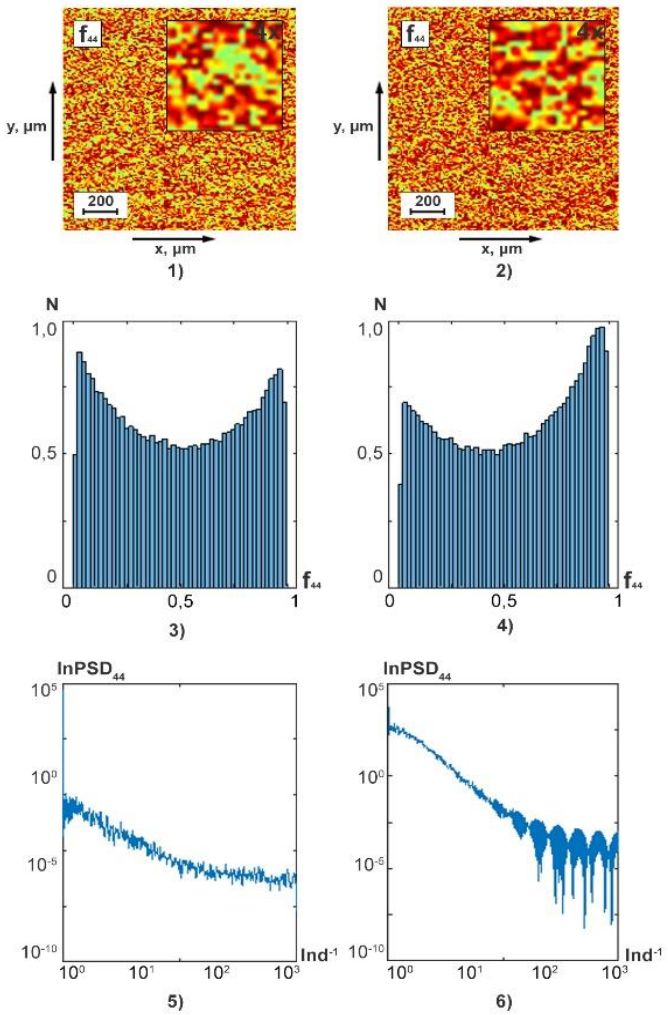

Fig. 2. Maps (fragments (1), (2)), histograms (fragments (3),(4)) and logarithmic dependences of power spectra (fragments (5),(6)) of distributions $f_{44}(\delta)$ of birefringent spleen networks. Explanations in the text.

Comparative analysis of the values of $Z_{i=1;2;3;4}$ averaged within statistically reliable representative samples of samples of histological sections of the spleen $Z_{i=1;2;3;4}\left(f_{44}(\delta)\right)$ and $Z_{i=1;2;3;4}\left(\varphi_k = {}^{\pi}/_{8}, f_{44}(\delta)\right)$.

Table 2. Accuracy of differential diagnosis of the prescription of mechanical spleen injury

MMI	$F^{f_{44}}(h_i)$		Ac_{12},%
	Group 1	Group 2	
Z_1	1.42±0.088	1.28±0.075	61.2
Z_2	0.69±0.047	0.61±0.038	61.2
Z_3	0.35±0.018	0.43±0.025	66.7
Z_4	0.41±0.024	0.54±0.031	71.4
MMI	$F^{f_{44}}(\varphi_k = {}^{\pi}/_{8}; h_i)$		Ac_{12},%
	Group 1	Group 2	
Z_1	0.54±0.028	0.48±0.025	66.7
Z_2	0.14±0.007	0.11±0.006	66.7
Z_3	0.75±0.038	0.84±0.045	71.4
Z_4	1.14±0.064	1.35±0.071	76.1

The difference from zero ($Z_{i=1;2;3;4}(f_{44}) \neq 0$) of all 1st – 4th order statistical moments that characterize the distributions of random values of phase invariants $f_{44}(\delta)$ at all depths of histological sections of the spleen.

Most sensitive to the phase changes (φ_k) of the depth of the biological tissue layer were the statistical moments of the 3rd and 4th orders, which characterize the asymmetry (Z_3) and the kurtosis (Z_4) of the distributions $f_{44}(m,n)$.

Here we distinguish two boundary values of the depth of phase scanning of histological sections of the spleen:

- the "maximum" is the diffuse component of the object field of the experimental sample;
- "minimal" is a single scattered component of the object field of an optically thin layer of a spleen tissue sample.

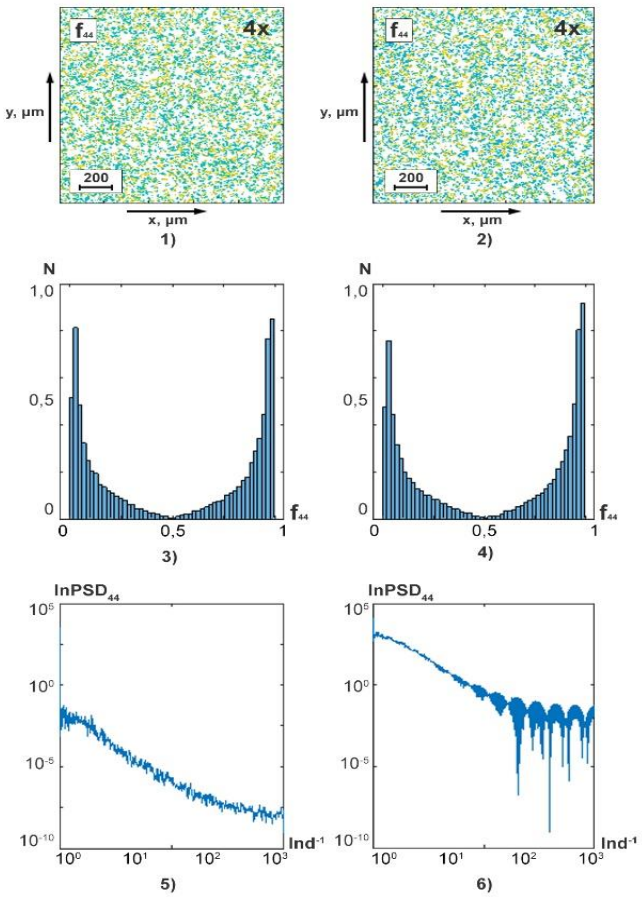

Fig. 3. Phase section $\varphi_k = {}^{\pi}/_{8}$ - Maps (fragments (1), (2)), histograms (fragments (3),(4)) and logarithmic dependences of power spectra (fragments (5),(6)) of distributions $f_{44}(\delta)$ birefringent networks of the spleen. Explanations in the text.

By the minimum phase depth, we will understand such a value $\varphi_{k_{min}}$, starting from which the values of the set of statistical moments of the 1st - 4th orders practically do not change, - $Z_{i=1;2;3;4}(\varphi_k, \omega_{ii}) \approx const$.

In our case, this mode begins to be implemented starting from $\varphi_{k_{min}} \leq {}^{\pi}/_{8}$.

We did not find significant intergroup differences. The maximum differences between the values of the 1st - 4th order statistical moments that characterize the phase matrix invariants of the optically anisotropic architectonics of spleen do not exceed 25% - 30%. As a result, the accuracy[50] of differential diagnosis of the prescription of mechanical injury is low - $Ac\left(Z_{i=3;4}(f_{44}(\delta))\right) \leq 71\% - 76\%$.

Based on this, we have considered the possibilities of a different, large-scale, self-similar approach to assessing the topographic structure of coordinate systems $f_{44}(m,n)$ and $f_{44}\left(\varphi_k = {}^{\pi}/_{8}, m, n\right)$.

6.1.2. Spleen – fractal analysis

As a first step, we used the well-known method [24, 25], which is based on approximating the logarithmic dependences of the power spectra of coordinate distributions of MMI. This fractal analysis of the topographic structure of the distributions $f_{44}(m,n)$ and $f_{44}\left(\varphi_k = {}^{\pi}/_{8}, m, n\right)$, which characterize the optically anisotropic architectonics of spleen, revealed signs of their multiscale self-similarity or multifractality. This fact is indicated by the presence of rectilinear ($100\mu m \leq d_i \leq 1000\mu m$) and curved ($1\mu m \leq d_i \leq 100\mu m$) slope sections of logarithmic dependencies $lnPSD_{44} - lnd^{-1}$, - Fig. 2, Fig. 3, fragments (3),(4).

From a physical point of view, this structure of $lnPSD_{44} - lnd^{-1}$ can be related to the fact that each fractal measure in the distributions $f_{44}(m,n)$ corresponds to a certain (partial) scale-self-like (with dimension h_j within $d_{min} \leq d_j \ll d_{max}$) set of the biological crystals.

The presence of dependence $lnPSD_{44} - lnd^{-1}$, oscillations may be due to the fact that in the process of formation of molecular complexes take part with statistically distributed birefringence parameters.

6.1.3. Multifractal analysis of spleen MMI

In Fig. 4 shows the lines of maximal modules (skeletons – "red dots" – maxima; "blue dots"- minima of wavelet coefficient amplitudes) wavelets coefficients of maps $W^{f_{44}}(a,b)$ (fragments (1),(3)) and multifractal spectra $F(h_i)$ of the $f_{44}(m,n)$ and $f_{44}\left(\varphi_k = {}^{\pi}/_{8}, m, n\right)$ (fragments (2),(4)). All results relate to the prescription of the mechanical injury of 6 hours.

Figure 5 shows similar results of the multifractal analysis of the distributions of $f_{44}(m,n)$ and $f_{44}\left(\varphi_k = {}^{\pi}/_{8}, m, n\right)$ for the limitation of mechanical injury is 24 hours.

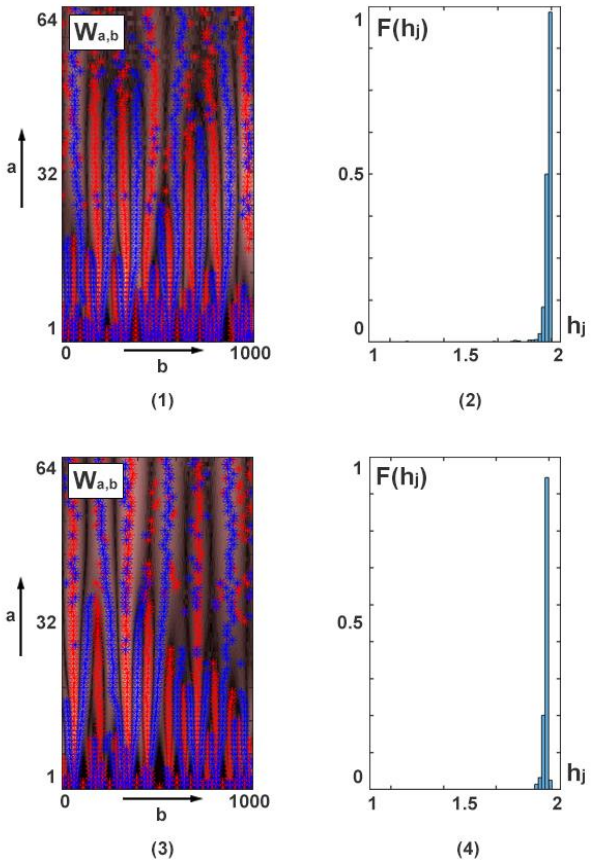

Fig. 4. Skeletons (fragments (1),(3)) and multifractal spectra $F^{f_{44}}(h_i)$ (fragments (2),(4)) of the phase $f_{44}(m,n)$ (fragments (1),(2)) and $f_{44}\left(\varphi_k = {}^{\pi}/_{8}, m, n\right)$ (fragments (3),(4)) Mueller matrix invariants of the histological section of the spleen - prescription of the mechanical injury of 6 hours.

A comparative analysis results of WTMM method revealed that:

- Optically anisotropic spleen component $f_{44}(m,n)$ and $f_{44}\left(\varphi_k = {}^{\pi}/_{8}, m, n\right)$ are characterized by a complex scale - like structure, which is characterized by individual multifractal spectra $F^{f_{44}}(h_i)$, - Fig. 4, Fig. 5 (fragments (2), (4)).
- The multifractal spectra $F^{f_{44}}(h_i)$ of MMI $f_{44}(m,n)$ and $f_{44}\left(\varphi_k = {}^{\pi}/_{8}, m, n\right)$ have an asymmetric structure with a clearly distinct extremum and a range of fractal dimension changes of $1.75 \lesssim h_i \lesssim 1.89$.
- For short-term (6 hours) injury of the spleen the multifractal spectra $F^{f_{44}}(h_i)$ are "narrower" and more asymmetric (Fig. 4, fragment (2),(4)) than similar multifractal spectral dependences $F^{f_{44}}(h_i)$, which are calculated for $f_{44}(m,n)$ for long-term (24 hours) (Fig. 5, fragments (2),(4)).

The fractal dimensions range Δh_i is larger for the spectrum $F^{f_{44}}(T = 24\,hours;\ h_i)$ than for $F^{f_{44}}(T = 6\,hours;\ h_i)$ - $\Delta h_i(24\,hous) > \Delta h_i(6\,hours)$. From a physical point of view, the results obtained can be linked to the following considerations. *First of all*. Each local optically anisotropic degree in the $f_{44}(m,n)$ and $f_{44}\left(\varphi_k = {}^{\pi}/_{8}, m, n\right)$ corresponds to its own value of the fractal dimension h_i, the probability and magnitude of which ($F(h_i)$) is determined by the specifics self-assembled crystallite complexes. *Second.* The highest probability of fractal dimension is inherent in the coordinate distributions $f_{44}\left(100\mu m \le d_{i(max)} \le 1000\mu m\right)$ of a spleen histological section.

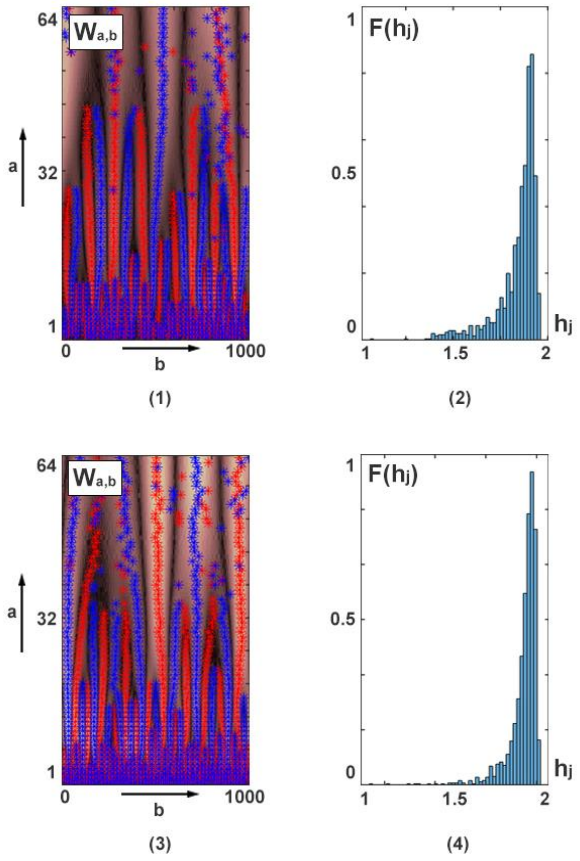

Fig. 5. Skeletons (fragments (1),(3)) and multifractal spectra $F^{f_{44}}(h_i)$ (fragments (2),(4)) of the phase $f_{44}(m,n)$ (fragments (1),(2)) and $f_{44}\left(\varphi_k = {}^{\pi}/_{8}, m, n\right)$ (fragments (3),(4)) Mueller matrix invariants of the histological section of the spleen - prescription of the mechanical injury of 24 hours.

Third. From the fractal geometry theory point of view, in the extreme case, the fibrillar network spatial orientation organization architectonics can lead to a straight line. For such situation, the multifractal spectrum degenerates into a delta function with the base value of the fractal dimension $h_{LB} \Rightarrow 1.0$. A different situation is realized for phase networks that form fractal measures in $f_{44}(\delta, m, n)$. Here, the boundary geometric situation is polycrystalline architectonics in the form of a plane, which corresponds to another value of the fractal dimension $h_{LB} \Rightarrow 2.0$. For a real physical situation, such trends are found in different localization multifractal spectra main extremes ($\max(F^{f_{44}}(h_i; T = 6\,hours))$ and $\max(F^{f_{44}}(h_i; T = 24\,hours))$). In this case, the fractal dimensions variation range Δh_i is larger for the spectrum $F^{f_{44}}(h_i; T = 24\,hours)$ than for $F^{f_{44}}(h_i; T = 6\,hours)$ - $\Delta h_i\left(f_{44}(T = 24\,hours; m, n)\right) > \Delta h_i\left(f_{44}(T = 6\,hours; m, n)\right)$.

A quantitative statistical estimate of multifractal spectra $F^{f_{44}}(h_i; T = 6\ hours)$ and $F^{f_{44}}(h_i; T = 24\ hours)$ is illustrated in Table 3.

Table 3. Accuracy of differential diagnosis of the prescription of mechanical spleen injury

MMI	$F^{f_{44}}(h_i)$		Ac_{12},%
	Group 1 ($T = 6\ hours$)	Group 2 ($T = 24\ hours$)	
Z_3	1.54±0.087	2.03±0.11	85.7
Z_4	2.33±0.12	3.41±0.16	90.4
MMI	$F^{f_{44}}(\varphi_k = {}^{\pi}/_{8}; h_i)$		Ac_{12},%
	Group 1 ($T = 6\ hours$)	Group 2 ($T = 24\ hours$)	
Z_3	2.27±0.13	3.11±0.15	90.4
Z_4	3.13±0.17	5.17±0.26	95.2

The analysis of the obtained results illustrates the high level of accuracy[50] of differential diagnosis of the prescription of mechanical injury using the technique of multifractal analysis of phase MMI optically anisotropic architectonics of histological sections of the spleen developed by us $Ac_{12}\left(\varphi_k = {}^{\pi}/_{8}, F^{f_{44}}(h_i)\right) = 95.2\%$.

7. Conclusions

In the linear birefringence approximation, a Mueller-matrix analytical description of the polarization properties of optically anisotropic architectonics of partially depolarizing preparations of spleen tissues is proposed.

By means of polarization-interference mapping and phase scanning of object fields of complex amplitudes of spleen tissue preparations reconstructed by digital holography, layered Mueller-matrix topographic maps of phase structure were obtained $f_{44}(m,n)$ and $f_{44}\left(\varphi_k = {}^{\pi}/_{8}, m, n\right)$ optically anisotropic architectonics of histological sections of spleen.

Comparative analysis of the values of statistical moments Z_i averaged within statistically reliable representative samples of samples of histological sections of the spleen $Z_{i=1;2;3;4}\left(f_{44}(\delta)\right)$ and $Z_{i=1;2;3;4}\left(\varphi_k = {}^{\pi}/_{8},\ f_{44}(\delta)\right)$ with varying degrees of mechanical injury did not find significant intergroup differences. The maximum differences between the values of the 1st - 4th order statistical moments that characterize the phase matrix invariants of the optically anisotropic architectonics of the spleen tissues do not exceed 25% - 30%.

Spleen tissue with different prescription of mechanical injury layer-by-layer multifractal properties were first demonstrated and studied using polarization-interference phase scaling by fractal analysis methods and maxima of wavelet transform modules complex application.

Analysis of the logarithmic dependences $lnPSD_{44} - lnd^{-1}$ of the power spectra of the spleen MMI $f_{44}(m,n)$ and $f_{44}\left(\varphi_k = {}^{\pi}/_{8}, m, n\right)$ revealed signs of a multifractal structure of the architectonics of their optically anisotropic polycrystalline networks - the presence of a set of linear sections (monofractal measures) of the approximating curve $H(\vartheta)$ for various geometric dimensions d_i.

A decrease in the value of the phase scanning parameter $\varphi_k \downarrow$ of the spleen MMI $f_{44}(m,n)$ and $f_{44}\left(\varphi_k = {}^{\pi}/_{8}, m, n\right)$ is accompanied by a decrease in the "number" and an increase in the "length" of linear sections of the approximating curve $H(\vartheta)$.

Within the wavelet transform maxima modules method, the following parameters are set:

individuality of multifractal spectra $F^{f_{44}}(h_i, \varphi_k)$ for spleen MMI, - $Z_{i=1;2;3;4}\left(F^{f_{44}}(T = 6\ hours;\ h_i)\right) \neq Z_{i=1;2;3;4}\left(F^{f_{44}}(T = 24\ hours;\ h_i)\right)$;

in all phase scaling φ_k planes of myocardium and brain, the following statistical relations take place $\begin{pmatrix} Z_{i=1;2}\left(F^{f_{44}}(T = 6\ hours;\ h_i)\right) < Z_{i=1;2}\left(F^{f_{44}}(T = 24\ hours;\ h_i)\right) \\ Z_{i=3;4}\left(F^{f_{44}}(T = 6\ hours;\ h_i)\right) < Z_{i=3;4}\left(F^{f_{44}}(T = 24\ hours;\ h_i)\right) \end{pmatrix}$.

The most sensitive, and therefore diagnostically promising, to changes of multifractal structure in the myocardium and brain MMI $f_{44}(m,n)$ and $f_{44}\left(\varphi_k = {}^{\pi}/_{8}, m, n\right)$ are the 3rd and 4th orders statistical moments. Its variation $\Delta Z_{3;4}^{f_{44}}(\varphi_k \downarrow)$ ranges lie in the range from 1.65 to 1.85 times.

The high applied biomedical efficiency WTMM algorithms is demonstrated – a high level of accuracy of differential diagnosis of the prescription of mechanical injury has been achieved using the technique of multifractal analysis of phase MMI optically anisotropic architectonics of histological sections of the spleen developed by us $Ac_{12}\left(\varphi_k = {}^{\pi}/_{8}, F^{f_{44}}(h_i)\right) = 95.2\%$;

Acknowledgment

Authors acknowledge the support from the National Research Foundation of Ukraine, Project 2022.01/0034; Scholarship of the Verkhovna Rada of Ukraine for Young Scientists-Doctors of Science 2023.

Conflict of Interest

The authors declare no conflict of interest.

Ethics Approval and Consent to Participate

This study was conducted in accordance with the principles of the Declaration of Helsinki, and in compliance with the International Conference on Harmonization-Good Clinical Practice and local regulatory requirements. Ethical approval was obtained from the Ethics Committee of the Bureau of Forensic Medicine of the Chernivtsi National University and the Bukovinian State Medical University (Chernivtsi, Ukraine).

References

[1] V. Shankaran, J. T. Walsh, Jr., and D. J. Maitland, “Comparative study of polarized light propagation in biological tissues,” J. Biomed. Opt. 7(3), 300–306 (2002).
[2] Valery V. Tuchin, Lihong Wang, Dmitry A. Zimnyakov, “Optical Polarization in Biomedical Applications,” in Biological and Medical Physics, Biomedical Engineering, Springer-Verlag Berlin Heidelberg, p.281, 2006.
[3] Tuchin, V. V. Tissue Optics: Light Scattering Methods and Instruments for Medical Diagnosis. Tissue Optics: Light Scattering Methods and Instruments for Medical Diagnosis: Third Edition (Society of Photo-Optical Instrumentation Engineers (SPIE) (2015).
[4] Ghosh, N. “Tissue polarimetry: concepts, challenges, applications, and outlook,” J. Biomed. Opt. 16, 110801 (2011).
[5] Jacques S. L. “Polarized light imaging of biological tissues,” in Handbook of Biomedical Optics2 (eds. Boas, D., Pitris, C. & Ramanujam, N.) 649–669, CRC Press, (2011).
[6] Layden D., Ghosh N. & Vitkin I. A. “Quantitative polarimetry for tissue characterization and diagnosis,” in Advanced Biophotonics: Tissue Optical Sectioning (eds. Wang, R. K. & Tuchin, V. V.) 73–108, CRC Press (2013).
[7] Vitkin A., Ghosh N. & de Martino A. “Tissue Polarimetry,” in Photonics: Scientific Foundations, Technology and Applications (ed. Andrews, D. L.) 239–321, John Wiley & Sons, Ltd. (2015).
[8] S. L. Jacques, R. J. Roman, and K. Lee, “Imaging superficial tissues with polarized light,” Lasers Surg. Med. 26, 119–129 (2000).
[9] L. V. Wang, G. L Coté, and S. L. Jacques, “Special section guest editorial: tissue polarimetry,” J. Biomed. Opt. 7, 278 (2002).
[10] H. R. Lee et al. "Digital histology with Mueller polarimetry and fast DBSCAN," Appl. Opt., 61(32) (2022).
[11] M. Kim et al. "Optical diagnosis of gastric tissue biopsies with Mueller microscopy and statistical analysis," J. Europ. Opt. Soc. Rapid Publ., 18(2), 10 (2022).
[12] H. R. Lee et al. "Digital histology with Mueller microscopy: how to mitigate an impact of tissue cut thickness fluctuations," J. Biomed. Opt. 24(7), 076004 (2019).
[13] P. Li et al. "Analysis of tissue microstructure with Mueller microscopy: logarithmic decomposition and Monte Carlo modeling," J. Biomed. Opt., 25(1), 015002 (2020).
[14] H. R. Lee et al "Mueller microscopy of anisotropic scattering media: theory and experiments", Proc. SPIE 10677, Unconventional Optical Imaging, 1067718 (2018)
[15] H. Ma, H. He, J. C. Ramella-Roman "Mueller matrix microscopy" In: J. C. Ramella-Roman, T. Novikova (Eds) Polarized Light in Biomedical Imaging and Sensing (Springer, Cham (2023).
[16] N. I. Zabolotna, S. V. Pavlov, et.al. “System of the phase tomography of optically anisotropic polycrystalline films of biological fluids,” SPIE Proc. 9166, 916616 (2014).
[17] R.K. Wang and V.V. Tuchin, eds, Advanced Biophotonics: Tissue Optical Sectioning, CRC Press, Taylor & Francis Group, London, p.681, 2013.
[18] A. Vitkin, N.Ghosh, and A. de Martino, “Tissue polarimetry” in Photonics: Scientific Foundations, Technology and Applications, D.L. Andrews, Ed., Vol. IV, pp. 239–321, John Wiley & Sons, Inc., Hoboken, New Jersey (2015).
[19] Yu. A. Ushenko, V. A. Ushenko, A. V. Dubolazov, V. O. Balanetskaya, N. I. Zabolotna, “Mueller-matrix diagnostics of optical properties of polycrystalline networks of human blood plasma,” Optics and Spectroscopy 112(6), 884-892 (2012).
[20] A.V. Dubolazov, N. V. Pashkovskaya, Yu. A. Ushenko, Yu. F. Marchuk, V. A. Ushenko, and O. Yu. Novakovskaya, "Birefringence images of polycrystalline films of human urine in early diagnostics of kidney pathology," Appl. Opt. 55, B85-B90 (2016).
[21] A.G. Ushenko, N.V. Pashkovskaya, O.V. Dubolazov, et al.: "Mueller Matrix Images of Polycrystalline Films of Human Biological Fluids," Romanian Reports in Physics, Vol. 67, No. 4, 1467-1479 (2015).
[22] M. S. Garazdyuk, V. T. Bachinskyi, O. Ya. Vanchulyak, et.al. “Polarization-phase images of liquor polycrystalline films in determining time of death,” Applied Optics, 55(12), B67-B71 (2016).
[23] Alexander Ushenko, Anton Sdobnov, Alexander Dubolazov, et.al. “Stokes-correlometry analysis of biological tissues with polycrystalline structure,” IEEE Journal of Selected Topics in Quantum Electronics 25/12 p. 1-12 (2018).

[24] Y. A. Ushenko, T. M. Boychuk, V. T. Bachynsky, et al., "Diagnostics of structure and physiological state of birefringent biological tissues: Statistical, correlation and topological approaches," in Handbook of Coherent-Domain Optical Methods: Biomedical Diagnostics, Environmental Monitoring, and Materials Science, V. V. Tuchin, Ed., 107–148, Springer New York, New York, NY (2013).
[25] Y. Ushenko, V. Balanetcka, et al., "Statistical, fractal, and singular processing of phase images of hominal blood plasma during the diagnostics of breast cancer," J. Flow Vis. Image Process. 18(3), 185–197 (2011).
[26] Y. O. Ushenko, Y. Y. Tomka, O. Pridiy, et al., "Wavelet analysis for mueller matrix images of biological crystal networks," Semicond. Phys. Quantum Electron. 12, 391–398 (2009).
[27] Y. Ushenko, Y. Tomka, O. Dubolazov, et al., "Wavelet-analysis for laser images of blood plasma," Adv. Electr. Comput. Eng. 11(2), 55–62 (2011).
[28] V. O. Ushenko "Spatial-frequency polarization phasometry of biological polycrystalline networks" Optical Memory and Neural Networks, 22(1), 56-64 (2013).
[29] V. A. Ushenko, N. D. Pavlyukovich, L. Trifonyuk, "Spatial-Frequency Azimuthally Stable Cartography of Biological Polycrystalline Networks," International Journal of Optics 2013, 7 (2013).
[30] VA Ushenko, AY Sdobnov, WD Mishalov, et.al. "Biomedical applications of Jones-matrix tomography to polycrystalline films of biological fluids," Journal of Innovative Optical Health Sciences, 12 (06), 1950017 (2019).
[31] AG Ushenko, OV Dubolazov, VA Ushenko, et.al. "Fourier polarimetry of human skin in the tasks of differentiation of benign and malignant formations," Applied Optics 55 (12), B56-B60 (2016).
[32] Ushenko O., Ushenko V., Besaha R., et al. "3D digital technology differentiation of high-quality and low-quality organic polymers," Proc. SPIE 12476, 124760F (2022).
[33] Peyvasteh, Motahareh, et al. "3D Mueller-matrix-based azimuthal invariant tomography of polycrystalline structure within benign and malignant soft-tissue tumours,"Laser Physics Letters" 17.11, 115606 (2020).
[34] Ushenko, Volodymyr A., et al. "3D Mueller matrix mapping of layered distributions of depolarization degree for analysis of prostate adenoma and carcinoma diffuse tissues." Scientific reports 11(1), 5162 (2021).
[35] Ushenko Volodimir, et al. "3D Mueller-matrix diffusive tomography of polycrystalline blood films for cancer diagnosis,"Photonics" 5 (4), (2018).
[36] Mandelbrot B B Fractals and Multifractals: Noise, Turbulence and Galaxies (New York: Springer+Verlag, 1989).
[37] O. V. Angelsky, A. Ushenko, Y. A. Ushenko, et al., "Statistical, correlation, and topological approaches in diagnostics of the structure and physiological state of birefringent biological tissues," in Handbook of Photonics for Biomedical Science, V. V. Tuchin, Ed., 283–322, CRC Press, Taylor and Francis Publishing, London (2010).
[38] O.V. Angelsky, A.G. Ushenko, Yu.A. Ushenko, V.P. Pishak, A.P. Peresunko, "Statistical, Correlation and Topological Approaches in Diagnostics of the Structure and Physiological State of Birefringent Biological Tissues," Handbook of Photonics for Biomedical Science, 283-322 (2010).
[39] Muzy J F, Bacry E, Arneodo A Int. J. Bifurcat. Chaos 4 245 (1994).
[40] Grassberger P Phys. Lett. A 97 227 (1983) 61. Grassberger P, Procaccia I Physica D 9 189 (1983).
[41] Hentschel H G E, Procaccia I Physica D 8 435 (1983).
[42] R.M.A.Azzam. Propagation of partially depolarized light through anisotropic media with or without depolarization. A differential 4x4 matrix calculus. J.Opt.Soc.Am., 68, 1756-1767, 1978.
[43] Oriol Arteaga and Adolf Canillas, "Analytic inversion of the Mueller-Jones polarization matrices for homogeneous media", Opt. Lett. 35, 559-561 (2010).
[44] Vladmir Z., Wang J.B., Yan X.H. Human Blood Plasma Crystal and Molecular Biocolloid Textures – Dismetabolism and Genetic Breaches. Natural Science journal – Xiangtan University, 2001,23,118-127.
[45] I. Daubechies, "Wavelets on the interval," in Progress in Wavelet Analysis and Applications: Proceedings of the International Conference" Wavelets and Applications," Toulouse, France June 1992, Y. Meyer and S. Roques, Eds., 95–107, Atlantica Seguier Frontieres (1993).
[46] M. Farge, "Wavelet transforms and their applications to turbulence," Annu. Rev. Fluid Mech. 24(1), 395–458 (1992).
[47] R. Marchesini, A. Bertoni, S. Andreola, et al., "Extinction and absorption coefficients and scattering phase functions of human tissues in vitro," Appl. Opt. 28(12), 2318–2324 (1989).
[48] D. K. Edwards, J. T. Gier, K. E. Nelson, et al., "Integrating sphere for imperfectly diffuse samples," J. Opt. Soc. Am. 51, 1279–1288 (1961).
[49] Goodman, J. W. Statistical Properties of Laser Speckle Patterns. (Springer, Berlin, Heidelberg, 1975).
[50] S. P. Robinson, Principles of forensic medicine, Cambridge University Press (1996).

Authors' Profiles

Oleksandr Ushenko, Professor at Chernivtsi National University, Head of Optics and Publishing Department. He received his BS and MS degrees in Optics from the Chernivtsi State University in 1975 and 1977, respectively, and his PhD degree in Optics and Laser Physics from the Chernivtsi State University in 1983. In 2000 he obtained D.Sc. in Optics and Laser Physics. He is the author of more than 200 journal papers, 60 patents and 20 monographies. His current research interests include laser polarimetry, polarization interferometry and digital holography.

Oleksandr Saleha, Postgraduate student at the Optics and Publishing Department of Chernivtsi National University. Research interests - digital processing of medical images using computer algorithms of statistical, correlation and fractal analysis.

Yuriy Ushenko was born on December 23, 1980 in Chishinau, Moldova. M.Sc. in Telecommunications (2003). PhD in Optics and Laser Physics (2006). D.Sc. in Optics and Laser Physics, Taras Shevchenko National University of Kyiv (2015). Current position – Professor, Head of Computer Science Department, Chernivtsi National University, Ukraine. Research Interests: Data Mining and Analysis, Computer Vision and Pattern Recognition, Optics & Photonics, Biophysics.

Ivan Gordey, Post-graduate student at the Computer Science Department of the Institute of Physical and Technical and Computer Sciences at the Yuri Fedkovich Chernivtsi National University. His research interests include digital processing of medical images using computer algorithms of statistical, correlation and fractal analysis.

Oleksandra Litvinenko, Postgraduate student at the Department of Forensic Medicine and Medicine Law, Bukovina State Medical University. Research interests - digital histological processing of medical images using computer algorithms of statistical, correlation and fractal analysis.

How to cite this paper: Oleksandr Ushenko, Oleksandr Saleha, Yurii Ushenko, Ivan Gordey, Oleksandra Litvinenko, "Multifractal Scaling of Singularity Spectra of Digital Mueller-matrix Images of Biological Tissues: Fundamental and Applied Aspects", International Journal of Image, Graphics and Signal Processing(IJIGSP), Vol.16, No.2, pp. 29-42, 2024. DOI:10.5815/ijigsp.2024.02.03